



Final results from DELPHI on neutral Higgs bosons in MSSM benchmark scenarios

V. Ruhlmann-Kleider
CEA, DSM/DAPNIA/SPP, Saclay

Abstract

The final interpretation of the results from DELPHI on the searches for MSSM Higgs bosons is presented in the framework of a few benchmark scenarios. The experimental results included encompass the searches for neutral Higgs bosons at LEP1 and LEP2 in final states as expected in the MSSM, as well as LEP2 searches for charged Higgs bosons and for neutral Higgs bosons decaying into hadrons. The theoretical scenarios are based on the currently most complete calculations of the radiative corrections at the two-loop order. Limits are derived on the masses of the lightest scalar and pseudoscalar Higgs bosons, h and A , and on $\tan\beta$. The dependence of these limits with the top quark mass is discussed.

Contributed Paper for LP 2005 (Uppsala) and HEP-EPS 2005 (Lisbon)

1 Introduction

This note presents the final interpretation of the results obtained by DELPHI on the searches for Higgs bosons in the whole data set recorded by the experiment. The theoretical framework is the Minimal Supersymmetric Standard Model (MSSM) which, as compared with the Standard Model, has an extended Higgs sector with two doublets of Higgs fields. Two important parameters in this sector are the Higgs doublet mixing angle, α , and the ratio of the doublet vacuum expectation values, $\tan\beta$. The two-doublets of Higgs fields lead to five physical Higgs bosons, of which three are neutral. In CP-conserving MSSM models, which is the case of the scenarios considered hereafter, two of the three neutral Higgs bosons, denoted h , for the lighter one, and H , are CP-even. The third one is a CP-odd pseudo-scalar, denoted A . In e^+e^- collisions, the dominant production mechanism for the CP-even scalars is the s-channel process described in Fig. 1 which is complemented by additional t-channel diagrams in the final states where a Higgs boson is produced with neutrinos or electrons, which proceed through W^+W^- and ZZ fusions, respectively. On the other hand, the CP-odd pseudo-scalar is produced in association with either of the CP-even scalars, as depicted in Fig. 1. Finally, charged Higgs bosons, H^+ and H^- , are also produced in pairs through a similar diagram.

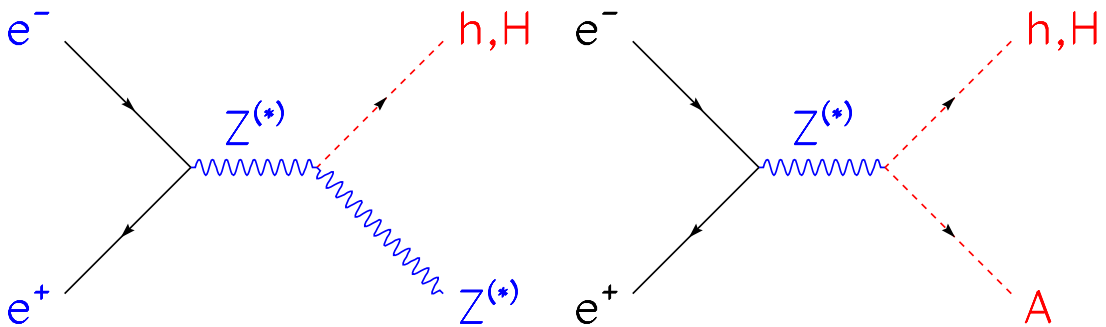


Figure 1: Main production processes of MSSM neutral Higgs bosons at LEP. Left: associated production of a Z and a CP-even Higgs boson. At LEP1, the intermediate Z is on-shell and the final Z is off-shell, while it is the reverse at LEP2. Right: pair-production of the CP-odd pseudo-scalar A and a CP-even Higgs boson. The exchanged Z is on-shell at LEP1.

In most of the MSSM parameter space, only hZ and hA productions are kinematically possible at LEP energies. These processes have complementary cross-sections since the hZZ and hAZ couplings are proportional to $\sin(\alpha - \beta)$ and $\cos(\alpha - \beta)$, respectively. If kinematically allowed, hZ production dominates at low $\tan\beta$ or at large m_A , while in the rest of the parameter space, it is suppressed with respect to hA pair-production. The third neutral Higgs boson, H , in some scenarios and in limited regions of the parameter space, is light enough and can be produced with a large HZ or HA cross-section. As the HZZ (resp. HAZ) coupling is proportional to $\cos(\alpha - \beta)$ (resp. $\sin(\alpha - \beta)$), HZ production, when allowed by kinematics, arises at large $\tan\beta$, and HA production at low $\tan\beta$. Similarly, charged Higgs bosons kinematically accessible at LEP2 energies are predicted in limited regions of the MSSM parameter space, typically when A is light, whatever $\tan\beta$. The

minimal value of the mass of such charged Higgs bosons is $60 \text{ GeV}/c^2$.

In the range of masses accessible at LEP - up to 120 (100) GeV/c^2 in m_h or m_H (m_A) - and in most of the MSSM parameter space of the scenarios studied hereafter, the main decays of the three neutral Higgs bosons are into the pair of heaviest fermions kinematically permitted. Below the $\mu^+\mu^-$ threshold, a Higgs boson would decay into $\gamma\gamma$ or e^+e^- pairs with a significant lifetime. Above the $\mu^+\mu^-$ threshold, the lifetime is negligible and Higgs bosons decay at the primary vertex. Up to $3 \text{ GeV}/c^2$ the main decays are into $\mu^+\mu^-$ pairs and then into hadronic channels with a large proportion of two-prong final states. Above $3 \text{ GeV}/c^2$ the dominant decays are successively into $c\bar{c}$, $\tau^+\tau^-$ and finally $b\bar{b}$ pairs for Higgs boson masses above $12 \text{ GeV}/c^2$. Besides these decays into fermions, there are also regions of the parameter space where one neutral Higgs boson can undergo cascade decays to a pair of Higgs bosons, as for example $h \rightarrow AA$. In some cases, this mode dominates over the decays into SM particles. Finally, above $60 \text{ GeV}/c^2$, charged Higgs bosons can decay either into the pair of heaviest fermions allowed by kinematics, that is into cs or $\tau\nu$ pairs, or into a W^*A pair if A is light.

These different decay channels define the topologies that were searched for to cover the MSSM parameter region kinematically accessible at LEP energies. Section 2 describes these topologies as well as the definition and a summary of the techniques related to confidence levels used in the statistical interpretation of the searches. Section 3 presents the definition of the eight CP-conserving MSSM benchmark scenarios studied in this note. Compared to our previous results [1], the theoretical calculations are identical, i.e. include all dominant two-loop order radiative corrections. But the set of experimental searches was enlarged and more MSSM scenarios were included. Results combining all searches are presented in section 4. Since the top quark mass has a significant impact on the predicted mass spectrum of the neutral Higgs bosons, and hence on the experimental exclusion limits, especially that on $\tan\beta$, results are derived for several values of this mass, namely: $m_{\text{top}} = 169.2, 174.3, 179.4$ and $183.0 \text{ GeV}/c^2$. The value of $179.4 \text{ GeV}/c^2$, closest to the present experimental measurement of $m_{\text{top}} = 178.0 \pm 4.3 \text{ GeV}/c^2$ [2], has been chosen as a reference to quote absolute mass and $\tan\beta$ limits, as well as in most of the exclusion plots.

2 Experimental results and confidence levels

The different analyses performed to search for neutral and charged Higgs bosons in the whole DELPHI data sample are summarised in Table 1 which lists the final states, mass ranges, data samples and the references for more details about the selections and their performance. As compared to the set of experimental inputs used in our previous interpretation of [1], that one contains in addition the charged Higgs analyses and the searches for neutral Higgs bosons decaying into hadrons of any flavour. These latter are expected to provide the experimental sensitivity in scenarios where the Higgs boson decays into $b\bar{b}$ pair vanish. As their mass coverage start at low mass, they also increase the experimental sensitivity to Higgs bosons below the $b\bar{b}$ threshold, a region otherwise covered only by analyses of subsets of the LEP1 data sample. The same holds for charged Higgs boson searches.

When scanning over the parameter space of a model, confidence levels are computed at each point to test the compatibility of data with the hypothesis of background only

\sqrt{s} (GeV)	final state	range (GeV/ c^2)	\mathcal{L} (pb $^{-1}$)	disc. info.	ref.
hZ with direct decays					
91.	Z \rightarrow e $^+$ e $^-$, $\mu^+\mu^-$	< 0.21	2.5	no	[3]
91.	(h \rightarrow V 0) (Z \rightarrow any)	< 0.21	2.5	no	[3]
91.	(h \rightarrow 2 prongs) (Z \rightarrow q \bar{q})	0.21 – 2.	0.5	no	[4]
91.	(h \rightarrow jet) (Z \rightarrow e $^+$ e $^-$, $\mu^+\mu^-$)	1. – 20.	0.5	no	[4]
91.	(h \rightarrow jet jet) (Z \rightarrow l $^+$ l $^-$, $\nu\bar{\nu}$)	> 12.	3.6	no	[5]
91.	(h \rightarrow jet jet) (Z \rightarrow e $^+$ e $^-$, $\mu^+\mu^-$, $\nu\bar{\nu}$)	> 35.	33.4	no	[6]
161.,172.	(h \rightarrow b \bar{b})(Z \rightarrow any), (h \rightarrow $\tau^+\tau^-$)(Z \rightarrow q \bar{q})	> 40.	19.9	1d	[13]
183.	(h \rightarrow b \bar{b})(Z \rightarrow any), (h \rightarrow $\tau^+\tau^-$)(Z \rightarrow q \bar{q})	> 55.	52.0	1d	[14]
189.	(h \rightarrow b \bar{b})(Z \rightarrow any), (h \rightarrow $\tau^+\tau^-$)(Z \rightarrow q \bar{q})	> 65.	158.0	2d	[15]
192.-208.	(h \rightarrow b \bar{b})(Z \rightarrow any)	> 12.	452.4	2d	[16, 17]
192.-208.	(h \rightarrow $\tau^+\tau^-$)(Z \rightarrow q \bar{q})	> 50.	452.4	2d	[16, 17]
189.-208.	(h \rightarrow hadrons)(Z \rightarrow any but $\tau^+\tau^-$)	> 4.	610.4	mix	[20]
hA with direct decays					
91.	4 prongs	> 0.4	5.3	no	[7]
91.	$\tau^+\tau^-$ hadrons	> 8.	0.5	no	[8]
91.	$\tau^+\tau^-$ jet jet	> 50	3.6	no	[9]
91.	b \bar{b} b \bar{b} , b \bar{b} c \bar{c}	> 30.	33.4	no	[10]
91.	$\tau^+\tau^-$ b \bar{b}	> 16.	79.4	no	[19]
91.	b \bar{b} b \bar{b}	> 24.	79.4	no	[18]
133.	b \bar{b} b \bar{b}	> 80.	6.0	no	[12]
161.,172.	b \bar{b} b \bar{b} , $\tau^+\tau^-$ b \bar{b}	> 80.	20.0	1d	[13]
183.	b \bar{b} b \bar{b} , $\tau^+\tau^-$ b \bar{b}	> 100.	54.0	1d	[14]
189.	b \bar{b} b \bar{b} , $\tau^+\tau^-$ b \bar{b}	> 130.	158.0	2d	[15]
192.-208.	$\tau^+\tau^-$ b \bar{b}	> 120.	452.4	2d	[16, 17]
192.-208.	b \bar{b} b \bar{b}	> 80.	452.4	2d	[16, 17]
189.-208.	$\tau^+\tau^-\tau^+\tau^-$	> 8.	570.9	1d	[18]
189.-208.	b \bar{b} b \bar{b}	> 24.	610.2	no	[18]
189.-208.	hadrons	> 8.	610.4	mix	[20]
hZ or hA with h \rightarrow AA cascade					
91.	Z \rightarrow q \bar{q}	< 0.21	16.2	no	[11]
91.	(AA \rightarrow V 0 V 0) (Z \rightarrow any but $\tau^+\tau^-$)	< 0.21	9.7	no	[11]
91.	(AA \rightarrow $\gamma\gamma$) (Z \rightarrow any or A \rightarrow $\gamma\gamma$)	< 0.21	12.5	no	[11]
91.	(AA \rightarrow 4 prongs) (Z \rightarrow any or A \rightarrow 2 prongs)	> 0.21	12.9	no	[11]
91.	(AA \rightarrow hadrons) (Z \rightarrow $\nu\bar{\nu}$ or A \rightarrow hadrons)	> 0.21	15.1	no	[11]
91.	(AA \rightarrow $\tau^+\tau^-\tau^+\tau^-$) (Z \rightarrow $\nu\bar{\nu}$ or A \rightarrow $\tau^+\tau^-$)	> 3.5	15.1	no	[11]
161.,172.	(AA \rightarrow any) (Z \rightarrow q \bar{q} , $\nu\bar{\nu}$ or A \rightarrow any)	> 20.	20.0	1d	[13]
183.	(AA \rightarrow b \bar{b} b \bar{b}) (Z \rightarrow q \bar{q})	> 12.	54.0	1d	[14]
192.-208.	(AA \rightarrow b \bar{b} b \bar{b} , b \bar{b} c \bar{c} , c \bar{c} c \bar{c}) (Z \rightarrow q \bar{q})	> 12.	452.4	2d	[16, 17]
192.-208.	(AA \rightarrow c \bar{c} c \bar{c}) (Z \rightarrow q \bar{q})	> 4.	452.4	2d	[19]
H $^+$ H $^-$					
189.-208.	$c\bar{s}c s$, $c s \tau \nu_\tau$, $W^* A \tau \nu_\tau$, $W^* A W^* A$	> 40.	610.4	2d	[21]
189.-208.	$\tau^+ \nu_\tau \tau^- \bar{\nu}_\tau$	> 40.	570.8	1d	[21]

Table 1: List of signals expected from MSSM Higgs bosons that were searched for in the DELPHI data sample. Indicated for each signal are the centre-of-mass energy, final-state, analysed mass range, integrated luminosity, level of discriminant information included in the confidence level estimates (none, one- or two-dimensional..) and the reference where details of the analysis are published. Here h means either of the two CP-even scalars. The mass range applies to m_h for hZ production, to m_h+m_A for hA production, to m_A for h \rightarrow AA processes and to m_{H^\pm} for H $^+$ H $^-$ production. When no upper bound is given, the limit given by kinematics or vanishing branching fractions must be understood.

and with that of background plus signal as expected from the model. These are calculated using a modified frequentist technique based on the extended maximum likelihood ratio [22] which has also been adopted by the LEP Higgs working group. The basis of the calculation is the likelihood ratio test-statistic, \mathcal{Q} :

$$\ln \mathcal{Q} = -S + \sum_i \ln \frac{s_i + b_i}{b_i}$$

where S is the total signal expected and s_i and b_i are the signal and background densities for event i . These densities are constructed using either only expected rates or also additional discriminant information, which can be one- or two-dimensional. Table 1 presents the level of discriminant information for each channel: LEP1 results are relying on rates only, while LEP2 results mix channels without or with discriminant information. As an example, in neutral Higgs boson channels with discriminant information, the first variable is the reconstructed Higgs boson mass in the hZ analyses and the sum of the reconstructed h and A masses in the hA analyses, while the second variable, if any, is channel-dependent, as specified in the references listed in the Table. Charged Higgs analyses use discriminant information in a similar way and the definition of their discriminant variables can be found in [21]. The searches for Higgs bosons decaying hadronically encompass analyses without or with 1d discriminant information together with analyses whose selections vary with the mass hypothesis. We refer the interested reader to [20] for more details.

The observed value of \mathcal{Q} is compared with the expected Probability Density Functions (PDFs) for \mathcal{Q} , which are built using Monte Carlo sampling under the assumptions that background processes only or that both signal and background are present. The confidence levels CL_b and CL_{s+b} are their integrals from $-\infty$ to the observed value of \mathcal{Q} . Systematic uncertainties in the rates of signal or background events are taken into account in the calculation of the PDFs for \mathcal{Q} by randomly varying the expected rates while generating the distribution [23], which has the effect of broadening the expected \mathcal{Q} distribution and therefore making extreme events seem more probable.

CL_b is the probability of obtaining a result as background-like or more so than the one observed if the background hypothesis is correct. Similarly, the confidence level for the hypothesis that both signal and background are present, CL_{s+b} , is the probability, in this hypothesis, to obtain more background-like results than those observed. The quantity CL_s is defined as the ratio of these two probabilities, CL_{s+b}/CL_b . It is not a true confidence level, but a conservative pseudo-confidence level for the signal hypothesis. All exclusions discussed hereafter use CL_s and require it to be 5% for an exclusion confidence of 95%. As using CL_s instead of CL_{s+b} is conservative, the rate of fake exclusions is ensured to be below 5% when CL_s is equal to 5%.

We refer the interested reader to [19] for more details about the handling of the experimental inputs prior to the confidence level calculations. The most important issues are the estimation of the expected signal and background densities from simulation, the use of a linear interpolation to estimate densities at masses, center of mass energies or $\tan \beta$ values not included in the simulation, the way non-independent channels are treated to ensure that only independent results are statistically combined, and the way the possible simultaneous production of the two CP-even scalar Higgs bosons, h and H , is accounted for. Note that in analyses with selections varying with the mass hypothesis, h and H signals cannot be combined in the way described in [19]. In that case, only that signal with the highest expected exclusion power is retained at each test point.

3 The benchmark scenarios

At tree level, the production cross-sections and the Higgs branching fractions in the MSSM depend on two free parameters, $\tan\beta$ and one Higgs boson mass, or, alternatively, two Higgs boson masses, e.g. m_A and m_h . Radiative corrections introduce additional parameters related to supersymmetry breaking. Hereafter, the usual assumption that some of them are identical at a given energy scale is made: hence, the SU(2) and U(1) gaugino mass terms are assumed to be unified at the so-called GUT scale, while the sfermion mass terms or the squark trilinear couplings are assumed to be unified at the EW scale. Within these assumptions, the parameters beyond tree level are: the top quark mass, the Higgs mixing parameter, μ , the common sfermion mass term at the EW scale, M_{susy} , the SU(2) gaugino mass term at the EW scale, M_2 , the gluino mass, $m_{\tilde{g}}$, and the common squark trilinear coupling at the EW scale, A . The U(1) gaugino mass term at the EW scale, M_1 , is related to M_2 through the GUT relation $M_1 = (5/3)\tan^2\theta_W M_2$. The radiative corrections affect the relationships between the masses of the Higgs bosons, with the largest contributions arising from the top/stop loops. As an example, the h boson mass, which is below that of the Z boson at tree level, increases by a few tens of GeV/ c^2 in some regions of the MSSM parameter space due to radiative corrections.

3.1 The scenarios

In the following, eight benchmark scenarios are considered, as suggested in Ref. [24]. The values of their underlying parameters are quoted in Table 2. The first three scenarios are those usually studied at LEP. They have been proposed to test the sensitivity of LEP to Higgs bosons with either masses close to the kinematical limit or decays difficult to detect. Similarly, the five other scenarios are aimed at testing the sensitivity of the Higgs boson searches at hadron colliders. It is thus interesting to establish the LEP constraints in such models too.

The first two scenarios, called the m_h^{max} scenario and the no-mixing scenario, differ only by the value of $X_t = A - \mu \cot\beta$, the parameter which controls the mixing in the stop sector, and hence has the largest impact on the mass of the h boson. The m_h^{max} scenario leads to the maximum possible h mass as a function of $\tan\beta$. The no-mixing scenario is its counterpart with vanishing mixing, leading to upper bounds on m_h which are at least 15 GeV/ c^2 lower than in the m_h^{max} scheme. These two scenarios are quite representative of the sensitivity of LEP since the mass limits obtained in these schemes with earlier results were only slightly reduced in more general parameter scans [25].

The third scenario, called the large μ scenario, has a large and positive value of μ and a relatively small value of $m_{\tilde{g}}$. It predicts at least one scalar Higgs boson with a mass within kinematic reach at LEP2 in each point of the MSSM parameter space. However, there are regions for which detecting such a Higgs boson is difficult because of vanishing branching fractions into b-quarks. The dominant decays in these regions being still into hadrons, the main analysis channels suffer from large backgrounds. This scenario was designed to test the sensitivity of LEP through analyses that could not benefit from the b-tagging capabilities of the experiments.

Among the five other benchmark scenarios, three are variants of the m_h^{max} and no-mixing scenarios. The sign of μ and that of the mixing parameter have been reversed in the two scenarios derived from the LEP m_h^{max} scenario. The changes in the Higgs boson

scenario	M_{susy} (GeV/ c^2)	M_2 (GeV/ c^2)	$m_{\tilde{g}}$ (GeV/ c^2)	μ (GeV/ c^2)	X_t (GeV/ c^2)
m_h^{max}	1000	200	800	-200	$2 M_{\text{susy}}$
no mixing	1000	200	800	-200	0
large μ	400	400	200	1000	-300
$m_h^{\text{max}}, \mu > 0$	1000	200	800	200	$2 M_{\text{susy}}$
$m_h^{\text{max}}, \mu > 0, X_t < 0$	1000	200	800	200	$-2 M_{\text{susy}}$
no mixing, $\mu > 0$, large M_{susy}	2000	200	800	200	0
gluophobic	350	300	500	300	-750
small α	800	500	500	$2.5 M_{\text{susy}}$	-1100

Table 2: Values of the underlying parameters for the eight representative MSSM scenarios scanned in this paper. Note that X_t is $A - \mu \cot \beta$. These scenarios have been studied for several values of the top mass quark, $m_{t_{\text{op}}} = 169.2, 174.3, 179.4$ and 183.0 GeV/ c^2 .

mass spectrum and properties are small. The sign of μ has been reversed and the value of M_{susy} has been doubled in the scenario derived from the no mixing scenario of LEP. The higher M_{susy} scale leads to a few GeV/ c^2 increase of the theoretical upper bound on m_h . The last two scenarios have been proposed to test potential difficult cases for the searches at hadron colliders. Hence, the gluophobic scenario presents regions where the main production channel at the LHC, gluon fusion, is suppressed due to cancellations between the top quark and stop quark loops in the production process. Finally, in the small α scenario, important decay channels at the Tevatron and at the LHC, $h \rightarrow b\bar{b}$ and $h \rightarrow \tau^+\tau^-$, are suppressed when α is small, which occurs at large $\tan \beta$ and moderate m_A with the chosen set of parameter values.

scenario	$m_{t_{\text{op}}} \text{ (GeV}/c^2\text{)}$			
	169.2	174.3	179.4	183.0
m_h^{max}	128.2	132.9	138.6	142.7
no mixing	112.8	115.5	118.2	120.3
large μ	106.1	108.0	110.1	111.6
$m_h^{\text{max}}, \mu > 0$	128.4	134.1	140.1	144.3
$m_h^{\text{max}}, \mu > 0, X_t < 0$	124.5	128.8	134.3	138.2
no mixing, $\mu > 0$, large M_{susy}	117.0	120.2	123.7	126.3
gluophobic	115.7	118.8	122.0	124.4
small α	118.5	122.2	126.2	129.1

Table 3: Maximal value of m_h (in GeV/ c^2) in the eight benchmark MSSM scenarios studied in this note, as a function of $m_{t_{\text{op}}}$. Radiative corrections include all dominant second-order loop terms [26]. The maximum value of m_h corresponds approximately to the minimum value of m_H .

In all scenarios, the radiative corrections have been computed with all dominant two-loop order terms included, in the Feynman-diagrammatic approach [26]. As an illustration of the different scenarios, Table 3 gives the maximum value of m_h allowed by theory in each of them, for the four values of $m_{t_{\text{op}}}$. At a given $m_{t_{\text{op}}}$ value, the three m_h^{max} scenarios

give the highest upper bounds on m_h , the positive μ scenario leading to the maximal value. The large μ scenario presents the lowest upper bound, followed in increasing order by the no mixing scenario, the gluophobic one, the no mixing scenario with positive μ and the small α scheme. The maximum value of m_h increases significantly with m_{top} . The effect is most important in the three m_h^{max} scenarios, and is much smaller in the others, especially in the large μ scheme. It must be noted that the maximum value of m_h corresponds approximately to the minimum value of m_H in regions of large HHZ couplings. Thus, apart in the three m_h^{max} scenarios, the H signal is expected to contribute to the experimental sensitivity, e.g. in all other scenarios for a top mass of 169.2 GeV/ c^2 and in the no mixing and large μ scenarios for a top mass of 179.4 GeV/ c^2 .

3.2 The procedure

In each scenario, a scan was performed over the MSSM parameters $\tan\beta$ and m_A . The range in m_A spans from 0.02 GeV/ c^2 up to 1 TeV/ c^2 . Values of m_A leading to unphysical negative mass squared values were removed from the scans. Such points are rather rare, except in the large μ , gluophobic and small α scenarios (see section 4). The range in $\tan\beta$ extends from the minimal value allowed in each scenario ¹ up to 50, a value chosen in the vicinity of the ratio of the top- and b-quark masses, which is an example of the large $\tan\beta$ hypothesis favoured in some constrained MSSM models [29]. The scan steps were 1 GeV/ c^2 in m_A and 0.1 in $\tan\beta$ in the regions where m_h varies rapidly with these parameters. At low m_A , where the decays modes change rapidly with the Higgs boson mass, values tested were 0.02, 0.1, 0.25, 0.5, 1.5 and 3 GeV/ c^2 .

At each point of the parameter space, the hZ, hA and H^+H^- cross-sections and the Higgs branching fractions were taken from databases provided by the LEP Higgs working group, Ref. [30], on the basis of the theoretical calculations in Ref. [26], completed by that in Ref. [31] for the charged Higgs boson branching fractions. The signal expectations in each channel were then derived from the theoretical cross-sections and branching fractions, the experimental luminosity and the efficiencies. If necessary, a correction was applied to account for different branching fractions of the Higgs bosons between the test point and the simulation (e.g. for the hZ process, the simulation was done in the SM framework).

As discussed in [19, 1], neutral Higgs bosons can have non-negligible widths at large $\tan\beta$ when m_A is above a few tens of GeV/ c^2 . In this region, the experimental sensitivity is dominated by the LEP2 hA analyses dedicated to standard MSSM final-states. To account for width effects in these channels, efficiencies derived from simulations with h and A widths below 1 GeV/ c^2 (see e.g. [17]) were applied for $\tan\beta < 30$ only. Above that value, efficiencies were linearly interpolated in $\tan\beta$ between the efficiencies from these simulations and those from simulations at $\tan\beta = 50$ where the Higgs boson widths exceed the experimental resolution (typically, 5 GeV/ c^2 on the sum of the Higgs boson masses). As the Higgs boson widths grow approximately linearly with $\tan\beta$ above 30, a linear interpolation is valid. The same holds for the discriminant information, for which the same interpolation software was used for the PDF interpolation in mass or centre-of-mass energy [19]. The hZ and HZ channels at large $\tan\beta$ are much less affected by width effects since in most of the regions where they possibly contribute, their width is below the experimental resolution, as shown in [1].

¹The minimal value of $\tan\beta$ is 0.7 in the large μ scenario and in the no mixing scenario with positive μ and 0.4 in all other schemes. Lower $\tan\beta$ values give rise to unphysical negative mass squared values.

4 Results

The regions of the MSSM parameter space excluded at 95% CL or more by combining the results of Table 1 are hereafter discussed in turn for each scenario. As a general statement valid in all scenarios, most of the exclusion is made by the searches for neutral Higgs bosons in final-states as expected from most MSSM models. The searches for neutral Higgs bosons decaying hadronically bring a gain in exclusion at high mass in the large μ scenario and, at low masses, in all other scenarios given their more complete coverage at low m_A . The charged Higgs boson searches complete the exclusion at low m_A since in that region these bosons become kinematically accessible at LEP2.

4.1 The m_h^{\max} scenario

The excluded regions in the $(m_h, \tan\beta)$, $(m_A, \tan\beta)$ and (m_h, m_A) planes are presented in Fig. 2 for a top mass value of $179.4 \text{ GeV}/c^2$. The inclusion of the searches for the heavy scalar, H, brings no change in the excluded regions since H is above LEP sensitivity in this scenario (see Table 3). Basically, the exclusion is made by the results in the hZ (hA) channels in the low (large) $\tan\beta$ region while they both contribute at intermediate values. As compared to our previous results of Ref. [1], direct Higgs boson searches leave no unexcluded hole any longer at low m_h and m_A . In Ref. [1] such a hole was excluded only by the limit on the Z partial width that would be due to new physics. Here, the hole is excluded independently by the searches for charged Higgs bosons, which in that region have a mass around $80 \text{ GeV}/c^2$, a branching fraction into fermions above 90% and a large production cross-section. Altogether, the above results thus establish the following 95% CL lower limits on m_h and m_A for $m_{\text{top}} = 179.4 \text{ GeV}/c^2$:

$$m_h > 89.7 \text{ GeV}/c^2 \quad m_A > 90.4 \text{ GeV}/c^2$$

for any value of $\tan\beta$ between 0.4 and 50. The expected median limits are $90.6 \text{ GeV}/c^2$ for m_h and $90.8 \text{ GeV}/c^2$ for m_A . The observed limit in m_A (m_h) is reached at $\tan\beta$ around 20 (10), in a region where both the hZ and hA processes contribute. Furthermore, for $m_{\text{top}} = 179.4 \text{ GeV}/c^2$ there is an excluded range in $\tan\beta$ between 0.9 and 1.4 (expected [1.0-1.4]) which is valid for any value of m_A between 0.02 and $1000 \text{ GeV}/c^2$.

The m_{top} dependence of the above limits was studied, as summarised in Table 4. The mass limits remain unchanged when varying m_{top} , for m_h is insensitive to m_{top} in the region of large $\tan\beta$ and intermediate m_A where the limits are set. On the other hand, the excluded range in $\tan\beta$ is governed by the maximal value of m_h , which is reached at large m_A where m_h is very sensitive to m_{top} , as illustrated in the top left-hand plot in Fig. 2: hence the variation of the limits in $\tan\beta$ as reported in Table 4 and Fig. 10. It must be noted that for a top mass of $183 \text{ GeV}/c^2$, there is no longer any exclusion in $\tan\beta$ in that scenario.

4.2 The m_h^{\max} scenarios with reverse signs of μ and X_t

The excluded regions in the $(m_h, \tan\beta)$, $(m_A, \tan\beta)$ and (m_h, m_A) planes for a top mass value of $179.4 \text{ GeV}/c^2$ are presented in Fig. 3 for the m_h^{\max} scenario with positive μ and in Fig. 4 for the m_h^{\max} scenario with positive μ and negative X_t . The results are quite similar to that in the previous scenario. The third neutral Higgs boson, H, being too heavy does

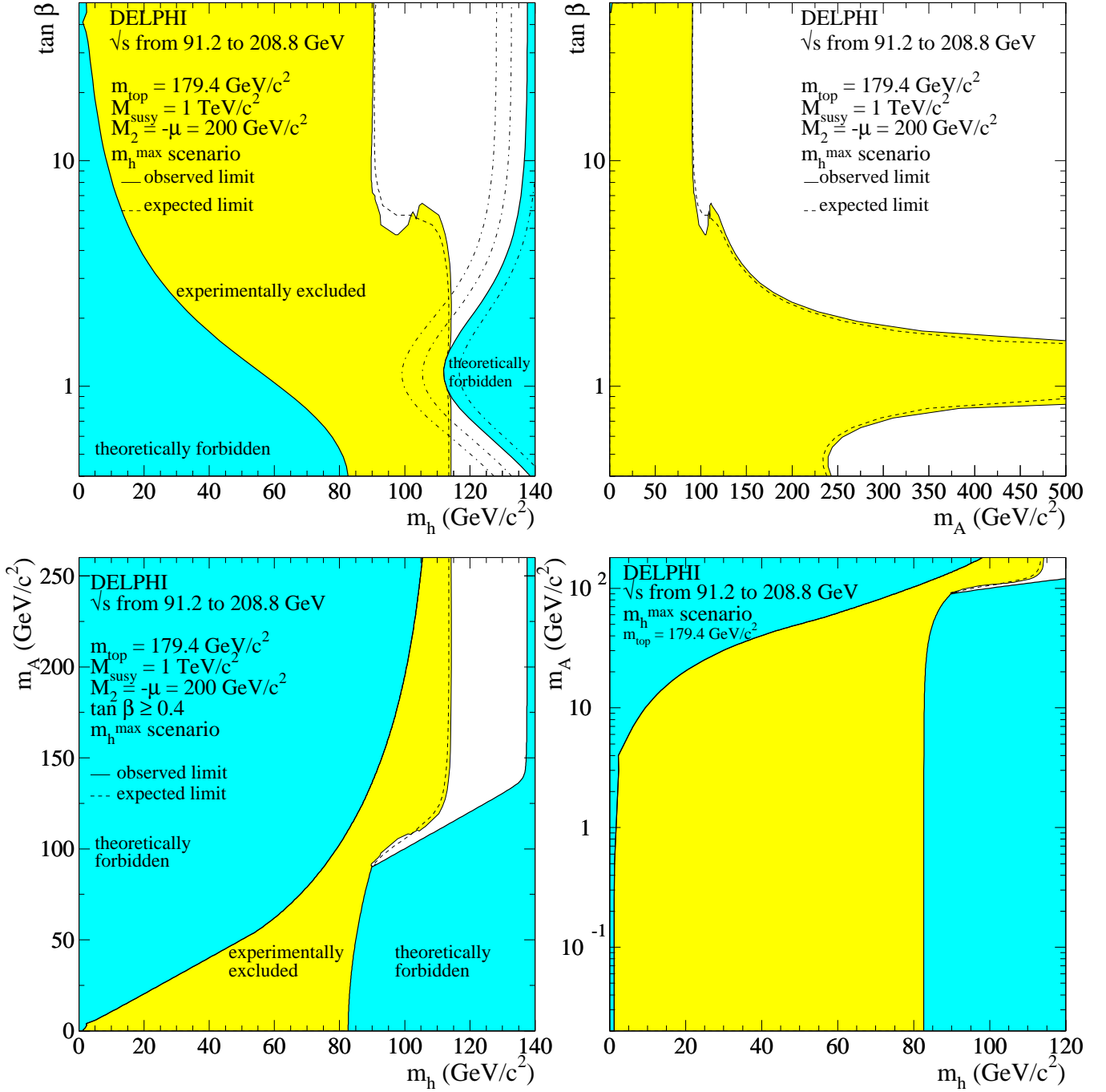


Figure 2: MSSM m_h^{\max} scenario: regions excluded at 95% CL by combining the results of the Higgs boson searches in the whole DELPHI data sample (light shaded area). The dashed curves show the median expected limits. The dark shaded areas are the regions not allowed by the MSSM model in this scenario. The dash-dotted lines in the top left-hand plot are the theoretical upper bounds for a top mass of 169.2, 174.3 and 183.0 GeV/c^2 (from left to right).

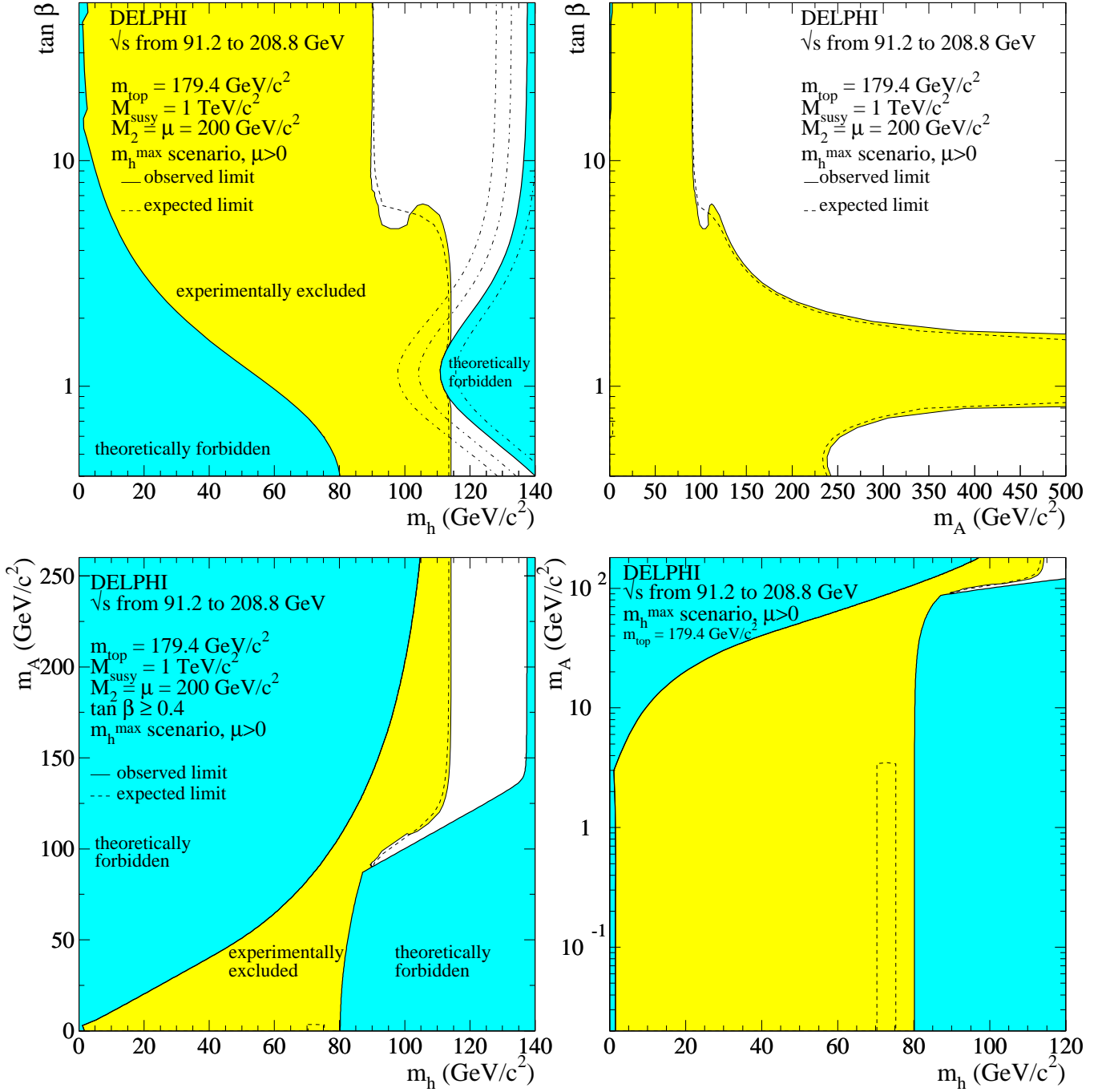


Figure 3: MSSM m_h^{\max} scenario with positive μ : regions excluded at 95% CL by combining the results of the Higgs boson searches in the whole DELPHI data sample (light shaded area). The dashed curves show the median expected limits. The dark shaded areas are the regions not allowed by the MSSM model in this scenario. The dash-dotted lines in the top left-hand plot are the theoretical upper bounds for a top mass of 169.2, 174.3 and 183.0 GeV/c^2 (from left to right).

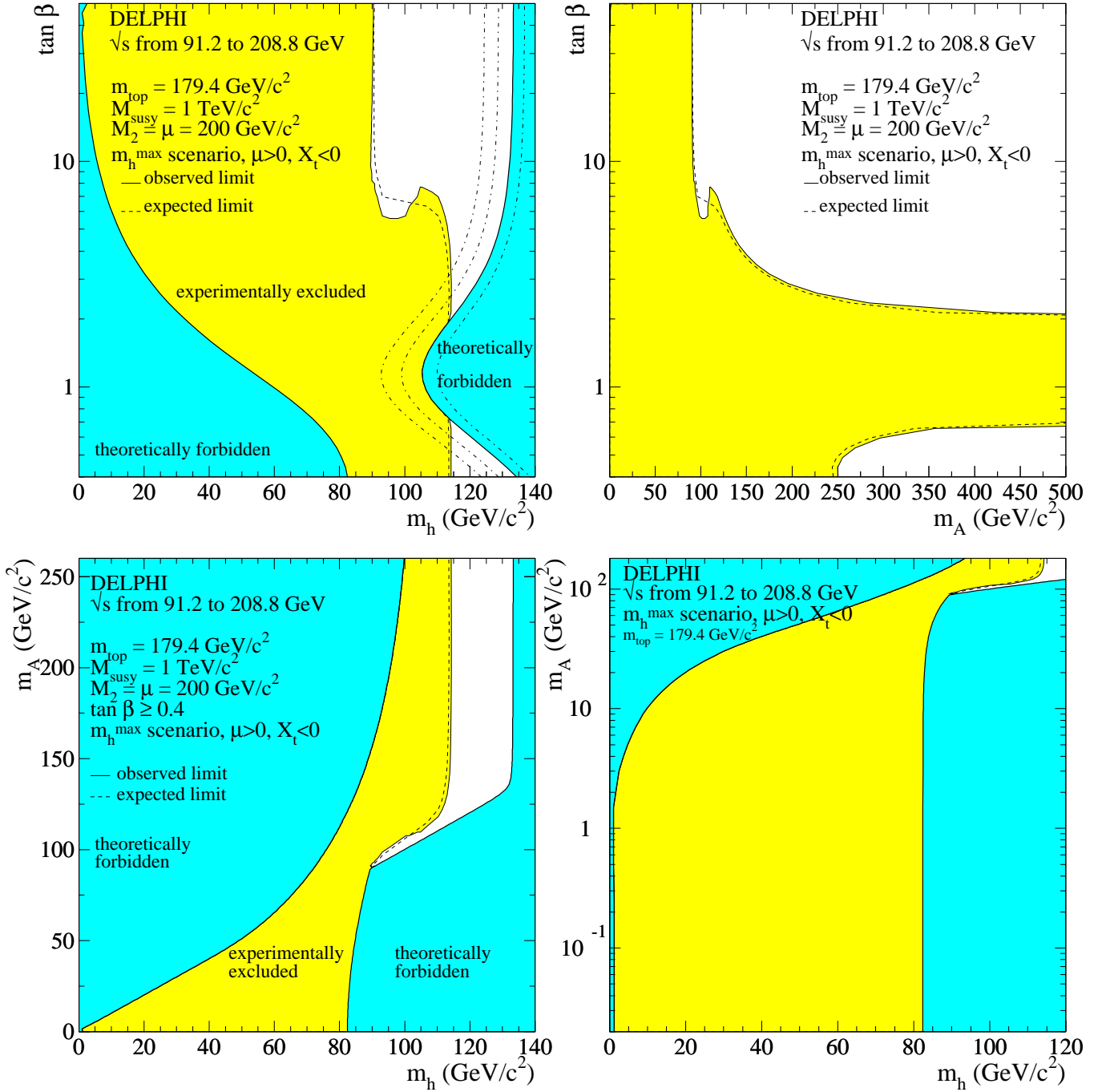


Figure 4: MSSM m_h^{\max} scenario with positive μ and negative X_t : regions excluded at 95% CL by combining the results of the Higgs boson searches in the whole DELPHI data sample (light shaded area). The dashed curves show the median expected limits. The dark shaded areas are the regions not allowed by the MSSM model in this scenario. The dash-dotted lines in the top left-hand plot are the theoretical upper bounds for a top mass of 169.2, 174.3 and 183.0 GeV/c^2 (from left to right).

not contribute and the charged Higgs channels provide a gain in exclusion at low m_h and m_A . Mass limits are within 200 MeV/ c^2 from that in the m_h^{\max} scenario and do not vary significantly with m_{top} , as reported in Table 4.

To compare observed and median limits, the 95% CL lower limits on m_h and m_A in the m_h^{\max} scenario with positive μ for $m_{\text{top}} = 179.4$ GeV/ c^2 are:

$$m_h > 89.5 \text{ GeV}/c^2 \quad m_A > 90.3 \text{ GeV}/c^2$$

for any value of $\tan\beta$ between 0.4 and 50. The expected median limits are 90.3 GeV/ c^2 for m_h and 90.4 GeV/ c^2 for m_A . The 95% CL lower limits on m_h and m_A in the m_h^{\max} scenario with positive μ and negative X_t for $m_{\text{top}} = 179.4$ GeV/ c^2 are:

$$m_h > 89.5 \text{ GeV}/c^2 \quad m_A > 90.4 \text{ GeV}/c^2$$

for any value of $\tan\beta$ between 0.4 and 50. The expected median limits are 90.4 GeV/ c^2 for m_h and 90.6 GeV/ c^2 for m_A .

On the other hand, the excluded ranges in $\tan\beta$ are different, since the three m_h^{\max} scenarios have different theoretical upper bounds on m_h . For $m_{\text{top}} = 179.4$ GeV/ c^2 the excluded range in $\tan\beta$ in the m_h^{\max} scenario with positive μ lies between 0.9 and 1.5 (expected [0.9-1.5]), while in the m_h^{\max} scenario with positive μ and negative X_t it spans from 0.7 to 1.9 (expected [0.7-1.9]). These limits are valid for any value of m_A between 0.02 and 1000 GeV/ c^2 . Note that despite the higher maximal value of m_h in the m_h^{\max} scenario with positive μ , the most conservative limits in $\tan\beta$ are still derived in the m_h^{\max} scenario, reflecting the differences in the theoretical upper bounds at $\tan\beta$ around 1 (see top left-hand plots in Fig. 2 and Fig. 3). The m_{top} dependence of the above limits is presented in Table 4 and Fig. 10. For a top mass of 183 GeV/ c^2 , there is no longer any exclusion in $\tan\beta$ in the m_h^{\max} scenario with positive μ , while there is still one in the scenario with positive μ and negative X_t due to the lower maximal value of m_h in that scenario.

4.3 The no mixing scenario

The excluded regions in the $(m_h, \tan\beta)$, $(m_A, \tan\beta)$ and (m_h, m_A) planes for a top mass value of 179.4 GeV/ c^2 are presented in Fig. 5. In this scenario, if the top is not too heavy, the heavy scalar, H, is kinematically accessible at large $\tan\beta$ and moderate m_A , the region where the mass limits in m_A and m_h are set. Thus, allowing for its production increases the sensitivity of the searches.

The zoom at low m_A in the (m_h, m_A) projection shows that there are three unexcluded holes below 4 GeV/ c^2 in m_A . The one at low m_h is similar to that encountered in the m_h^{\max} scenarios. As compared to our previous results of Ref. [1], this hole is almost fully excluded by the searches for charged Higgs bosons. A tiny region close to the theoretical lower bound on m_h remains unexcluded by the direct Higgs boson searches. However, the limit on the Z partial width that would be due to new physics [32], $\Gamma^{\text{new}} < 6.6$ MeV/ c^2 , translates, when applied to the hA process, into an excluded region that encompasses that area. The two other unexcluded regions have $\tan\beta$ below 1.0 and m_h between 59 and 82 GeV/ c^2 . In that region, m_A is below the kinematic threshold $m_h = 2m_A$, the decay $h \rightarrow AA$ opens and can supplant the $h \rightarrow b\bar{b}$ mode. Our LEP2 $h \rightarrow AA$ searches, covering A masses above the $c\bar{c}$ threshold (see Table 1), have no sensitivity

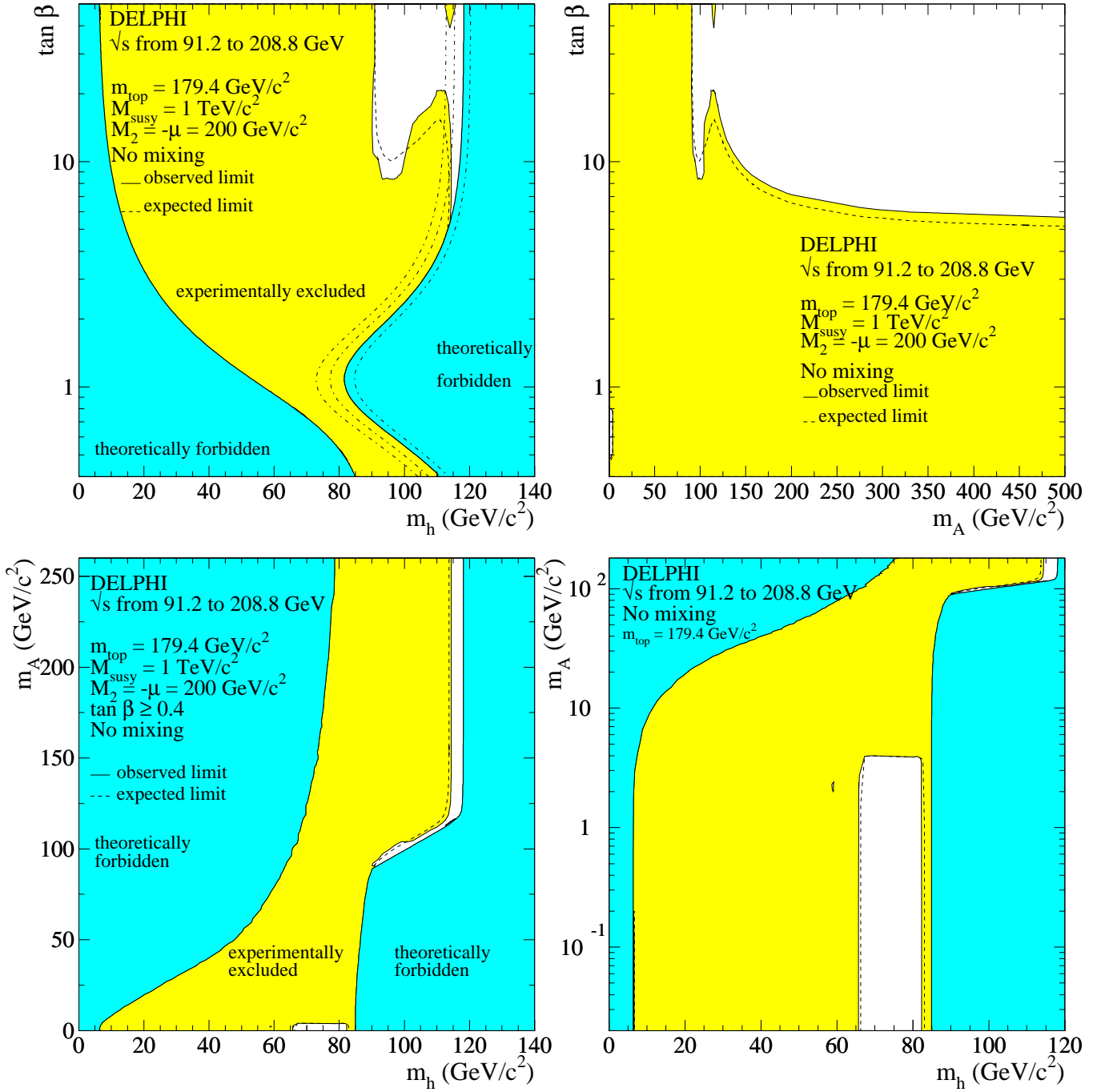


Figure 5: MSSM no-mixing scenario: regions excluded at 95% CL by combining the results of the Higgs boson searches in the whole DELPHI data sample (light shaded area). There are three unexcluded regions at low m_A , which are too small to be visible in the top left-hand plot. The one at low m_A and m_h is fully excluded by the limit on the Z partial width that would be due to new physics [32]. The dashed curves show the median expected limits. The dark shaded areas are the regions not allowed by the MSSM model in this scenario. The dash-dotted lines in the top left-hand plot are the theoretical upper bounds for a top mass of 169.2, 174.3 and 183.0 GeV/c² (from left to right).

there. Similarly, charged Higgs bosons, although kinematically accessible with a mass between 65 and 80 GeV/ c^2 , have a large branching fraction into W^*A . As our charged Higgs boson searches in these channels assume m_A above 12 GeV/ c^2 (see Table 1), the overall experimental sensitivity in that region remains weak and no exclusion at 95% CL can be derived (the maximum value of CL_s there is 25%). Note that the nearby region with m_h from 82 GeV/ c^2 to the theoretical upper bound on m_h is excluded at 95% CL by the charged Higgs boson searches through their fermionic decays which dominate the W^*A mode there.

The above results thus establish the following 95% CL lower limits on m_h and m_A for $m_{\text{top}} = 179.4$ GeV/ c^2 :

$$m_h > 90.0 \text{ GeV}/c^2 \quad m_A > 90.8 \text{ GeV}/c^2$$

for any value of $\tan\beta$ between 0.96 and 50. The expected median limits are 90.8 GeV/ c^2 for m_h and 90.7 GeV/ c^2 for m_A . The observed limits in m_A and m_h are reached at $\tan\beta$ around 15, in a region where both the hZ and hA processes contribute. Furthermore, there are excluded ranges in $\tan\beta$, the largest interval for $m_{\text{top}} = 179.4$ GeV/ c^2 being between 1.0 and 5.4 (expected [0.8-4.9]) which is valid for any value of m_A between 0.02 and 1000 GeV/ c^2 .

The m_{top} dependence of the above limits was studied, as shown in Table 4 and Fig. 10. In this scenario, both the mass limits and the excluded range in $\tan\beta$ change when varying m_{top} . Indeed, as already mentioned, the mass limits in m_A and m_h rely on the searches for H , whose mass is very sensitive to m_{top} in the region where the limits are set. Similarly, the maximal value of m_h , which governs the limits in $\tan\beta$, is reached at large m_A where m_h is very sensitive to m_{top} (see Table 3). Note that for a top mass of 169 GeV/ c^2 , m_H decreases by 3 GeV/ c^2 in the region where the mass limits are set, making the H signal more within the sensitivity of LEP2: the whole parameter space of the no mixing scenario is then accessible and found to be excluded at 95% CL, apart from a hole at $\tan\beta$ below 1.0 and m_A below 4 GeV/ c^2 , which is disfavoured at 75% CL only.

4.4 The no mixing scenario with positive μ and large M_{susy}

The excluded regions in the $(m_h, \tan\beta)$, $(m_A, \tan\beta)$ and (m_h, m_A) planes for a top mass value of 179.4 GeV/ c^2 are presented in Fig. 6. The larger M_{susy} makes the impact of the H signal, and hence the exclusion limits, weaker than in the previous scenario. On the other hand, the results in the low mass region, at m_A below 4 GeV/ c^2 , are similar to that in the no mixing scenario. The direct searches leave a tiny unexcluded region at low m_h which is excluded by the limit on Γ^{new} . A second region, at m_h between 65 and 72 GeV/ c^2 , remains unexcluded even when charged Higgs boson searches are included, due to the large branching fraction into W^*A decays, which are not covered by these searches at such low A masses. An exclusion at 85% CL is however achieved in this region.

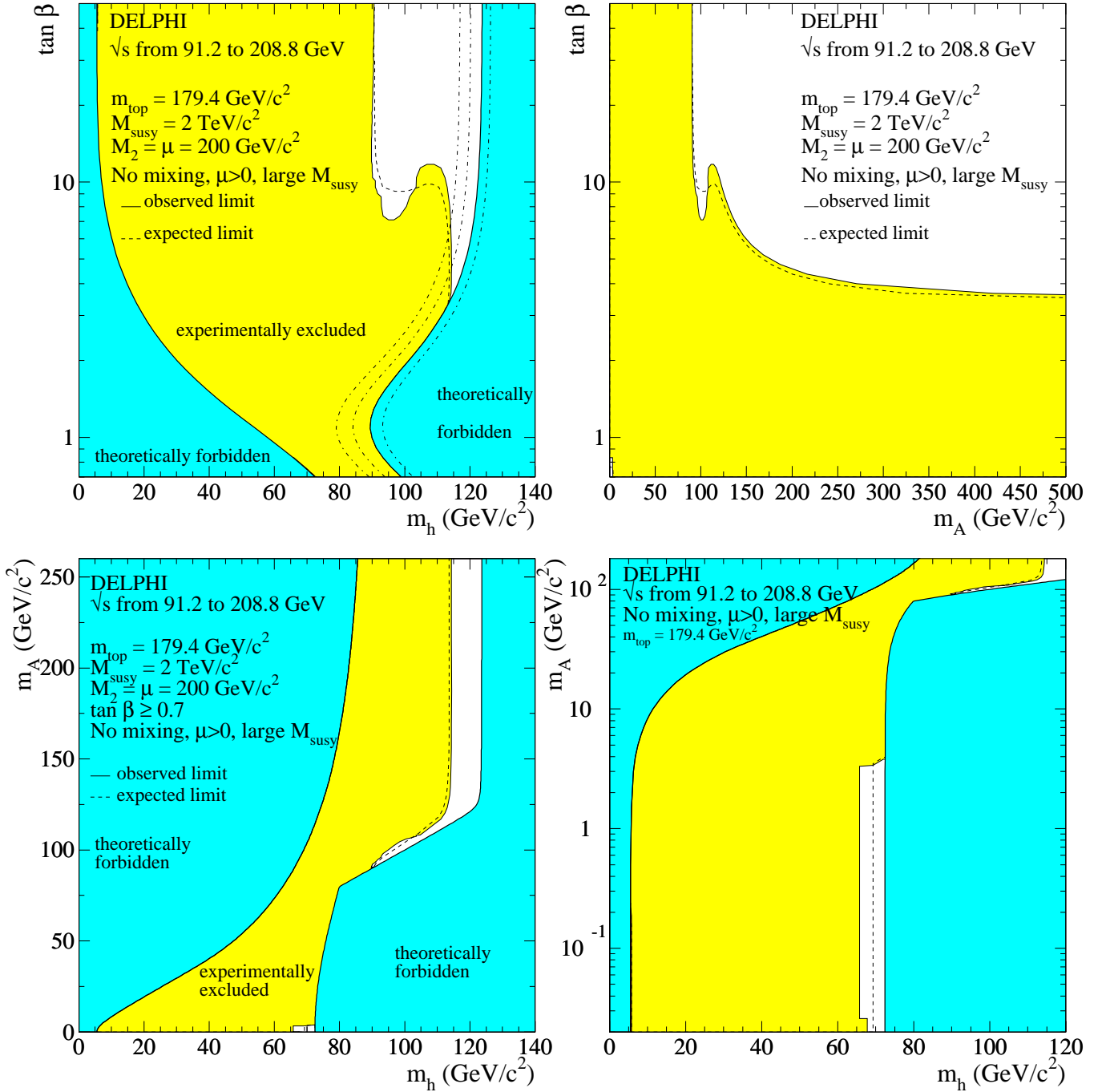


Figure 6: MSSM no-mixing scenario with positive μ and large M_{susy} : regions excluded at 95% CL by combining the results of the Higgs boson searches in the whole DELPHI data sample (light shaded area). There are two unexcluded regions at low m_A , which are too small to be visible in the top left-hand plot. The one at low m_A and m_h is fully excluded by the limit on the Z partial width that would be due to new physics [32]. The dashed curves show the median expected limits. The dark shaded areas are the regions not allowed by the MSSM model in this scenario. The dash-dotted lines in the top left-hand plot are the theoretical upper bounds for a top mass of 169.2, 174.3 and 183.0 GeV/c^2 (from left to right).

The above results thus establish the following 95% CL lower limits on m_h and m_A for $m_{\text{top}} = 179.4 \text{ GeV}/c^2$:

$$m_h > 89.7 \text{ GeV}/c^2 \quad m_A > 90.4 \text{ GeV}/c^2$$

for any value of $\tan\beta$ between 0.88 and 50. The expected median limits are $90.5 \text{ GeV}/c^2$ for both m_h and m_A . For $m_{\text{top}} = 179.4 \text{ GeV}/c^2$ there is an excluded range in $\tan\beta$ between 0.9 and 3.4 (expected [0.8-3.3]) which is valid for any value of m_A between 0.02 and $1000 \text{ GeV}/c^2$.

The m_{top} dependence of the above limits is presented in Table 4 and Fig. 10. The mass limits vary only slightly with m_{top} , since in the region where these are set, m_h is insensitive to m_{top} while m_H , although sensitive to m_{top} , is very close to the kinematic limit. Note also that, contrary to the case of the no mixing scenario, even for a top mass of $169 \text{ GeV}/c^2$ the parameter space of this scenario is not fully accessible, due to too high an upper (resp. lower) bound on m_h (resp. m_H). The exclusion is thus much weaker than in the no mixing scheme.

4.5 The large μ scenario

The excluded regions in the large μ scenario are presented in the $(m_h, \tan\beta)$ and $(m_A, \tan\beta)$ planes in Fig. 7 for values of the top quark mass of 174.3 and $179.4 \text{ GeV}/c^2$. In these figures, the contribution of the H signal and that of the searches for neutral Higgs bosons decaying into hadrons of any flavour are highlighted.

A large fraction of the allowed domain is excluded by the searches for the h, A and H Higgs bosons into standard MSSM final states. In particular, given that the theoretical upper bound on the h boson mass in that scenario is low (around $110.0 \text{ GeV}/c^2$, see Table 3), the sensitivity of the hZ channels is high even at large $\tan\beta$, which explains why the excluded region reaches the theoretically forbidden area for large values of $\tan\beta$. As the value of the upper bound on m_h is also the theoretical lower bound on m_H at large $\tan\beta$, allowing for the production of H translates into a significant gain in exclusion. The searches for neutral Higgs boson into hadrons of any flavour brings an additional exclusion in regions left unexcluded by the standard searches at $\tan\beta$ above 10. At moderate m_A , hZ and hA productions are low due to weak hZZ couplings for hZ and to kinematics for hA. On the other hand, HZ production is large but H is decoupled from $b\bar{b}$. At larger m_A , hA and HZ productions are kinematically forbidden, hZ production is large but the $h \rightarrow b\bar{b}$ branching fraction vanishes. In both cases, the Higgs boson whose production is allowed (H or h) has a large branching fraction into hadrons and a mass close to the sensitivity of our searches for neutral Higgs boson decaying into hadrons and fully coupled to the Z. This explains why these searches lead to an additional but only partial exclusion in these regions. Note that increasing the top quark mass from 174.3 to $179.4 \text{ GeV}/c^2$ leads to larger an unexcluded area, for there are more points with vanishing h or H branching fractions into $b\bar{b}$ and, as m_h and m_H increase with m_{top} , the impact of the searches for hadronically decaying Higgs bosons becomes also weaker. However, when combining the four LEP experiments, the sensitivity of these searches increases and becomes high enough to cover almost entirely these regions of vanishing branching fractions into $b\bar{b}$ [30].

At low masses, there is one unexcluded tiny hole at low m_A and $\tan\beta$ above 1, which is due to the lack of searches for the topology with two jets and hadrons as expected

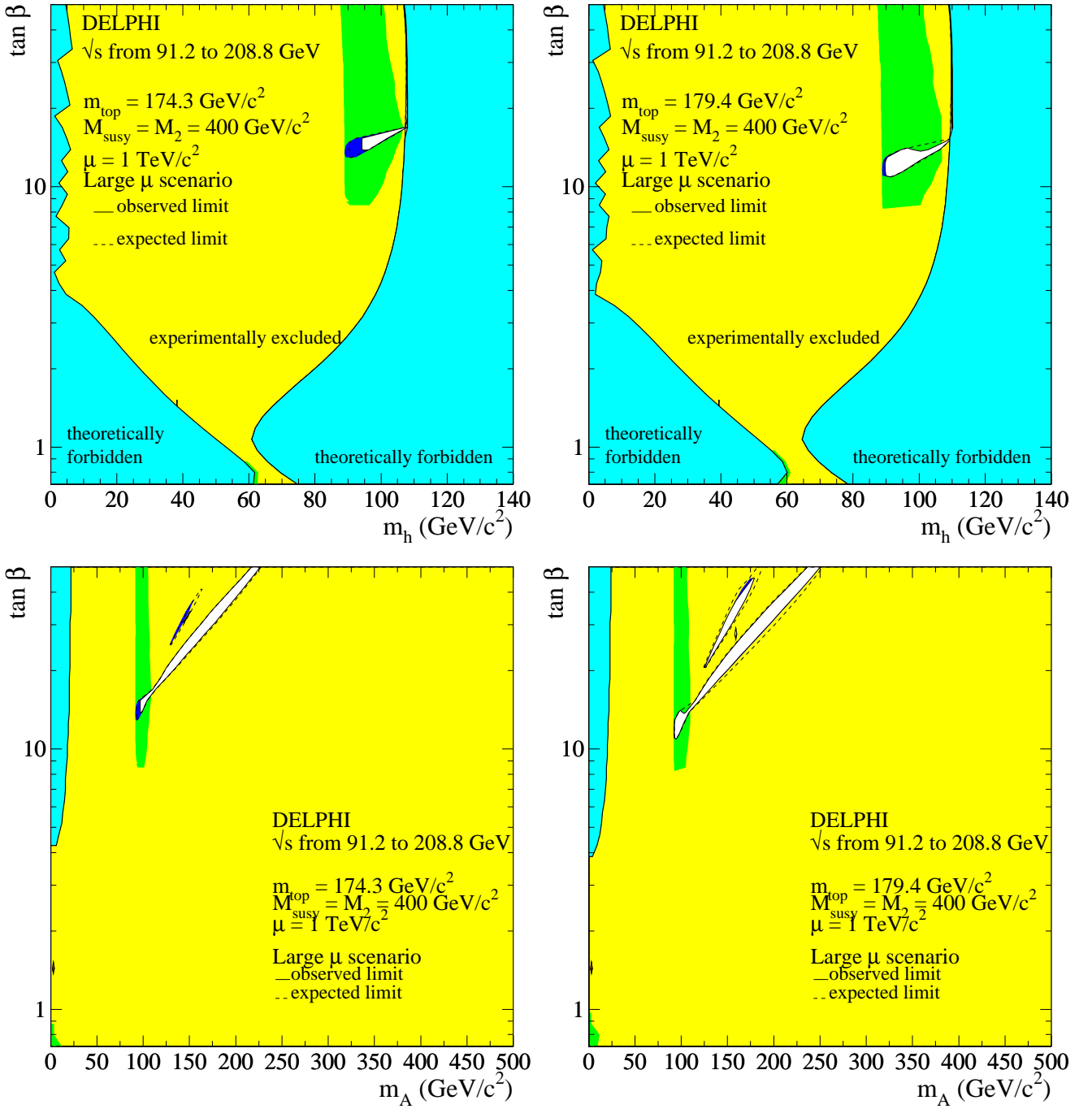


Figure 7: MSSM large μ scenario: regions excluded at 95% CL by combining the results of the Higgs boson searches in the whole DELPHI data sample (light shaded and embedded dark shaded areas). Results are shown for two values of the top mass, 174.3 and 179.4 GeV/c^2 . The embedded dark shaded areas are excluded by the searches for the heavy scalar Higgs boson, H (green) and by that for neutral Higgs bosons decaying into hadrons (dark blue). The unexcluded hole at low m_A and $\tan \beta$ above 1 is excluded by the limit on the Z partial width [32] that would be due to new physics (red). The dashed curves show the median expected limits. The dark shaded areas with bold contours are the regions not allowed by the MSSM model in this scenario. Note in particular the large forbidden region in the $(m_A, \tan \beta)$ projections, due to points leading to unphysical h masses.

from the hA process with one Higgs boson of mass above the $b\bar{b}$ threshold and the other one with a mass between 1 and 4 GeV/c². This point is excluded by the limit on Γ^{new} . All similar unexcluded holes at low masses present in our previous results [1] are now excluded either by the searches for neutral Higgs bosons decaying into hadrons or by the searches for charged Higgs bosons.

4.6 The gluophobic scenario

The excluded regions in the $(m_h, \tan\beta)$, $(m_A, \tan\beta)$ and (m_h, m_A) planes for a top mass value of 179.4 GeV/c² are presented in Fig. 8. Although this scenario was designed to test Higgs boson searches at hadron colliders, that is a phenomenology very different from that of LEP, results are similar to those derived in the previous scenarios. The shape of the excluded region is made by the results in the hZ (hA) channels in the low (large) $\tan\beta$ region while they both contribute at intermediate values. At low mass, the direct searches leave one unexcluded hole, below 4 GeV/c² in m_A and at $\tan\beta$ around 0.6, which is excluded by the limit on Γ^{new} .

The above results establish the following 95% CL lower limits on m_h and m_A for $m_{\text{top}} = 179.4$ GeV/c²:

$$m_h > 86.4 \text{ GeV}/c^2 \quad m_A > 93.2 \text{ GeV}/c^2$$

for any value of $\tan\beta$ between 0.4 and 50. The expected median limits are 86.6 GeV/c² for m_h and 93.3 GeV/c² for m_A . The observed limits in m_A and m_h are reached at $\tan\beta$ around 50, in a region where only the hA process contributes. Contrary to the other scenarios, the h and A bosons are not degenerate in mass at large $\tan\beta$, which reflects in the significant difference between the h and A mass limits. Furthermore, for $m_{\text{top}} = 179.4$ GeV/c², there is an excluded range in $\tan\beta$, between 0.5 and 3.7 (expected [0.5-3.6]) which is valid for any value of m_A between 0.02 and 1000 GeV/c².

The m_{top} dependence of the above limits is shown in Table 4 and Fig. 10. As already mentioned, the h and A bosons are not degenerate at large $\tan\beta$ and moderate m_A , the region where the mass limits are set. As a consequence, the value of m_h at fixed m_A and $\tan\beta$ is observed to vary significantly with m_{top} in that region. This is the main reason of the variations of the mass limits with m_{top} , an additional effect being the variations of m_H which is kinematically accessible at low m_{top} in this scenario (see Table 3). On the other hand, the variation of the excluded range in $\tan\beta$ is due, as in the other scenarios, to the change in the maximal value of m_h which is reached at large m_A where m_h is very sensitive to m_{top} .

4.7 The small α scenario

The excluded regions in the $(m_h, \tan\beta)$, $(m_A, \tan\beta)$ and (m_h, m_A) planes for a top mass value of 179.4 GeV/c² are presented in Fig. 9. The small α scheme is the second example of a scenario aiming at testing potential difficult cases for the Higgs boson searches at hadron colliders. As mentioned in section 3, this scenario presents regions of the parameter space where the $h \rightarrow b\bar{b}$ and $h \rightarrow \tau^+\tau^-$ decays vanish, which could be a problem at LEP too. The results in Fig. 9, similar to those derived in the previous scenarios, show that this is not the case. The reason is that at large $\tan\beta$, in the region accessible at LEP,

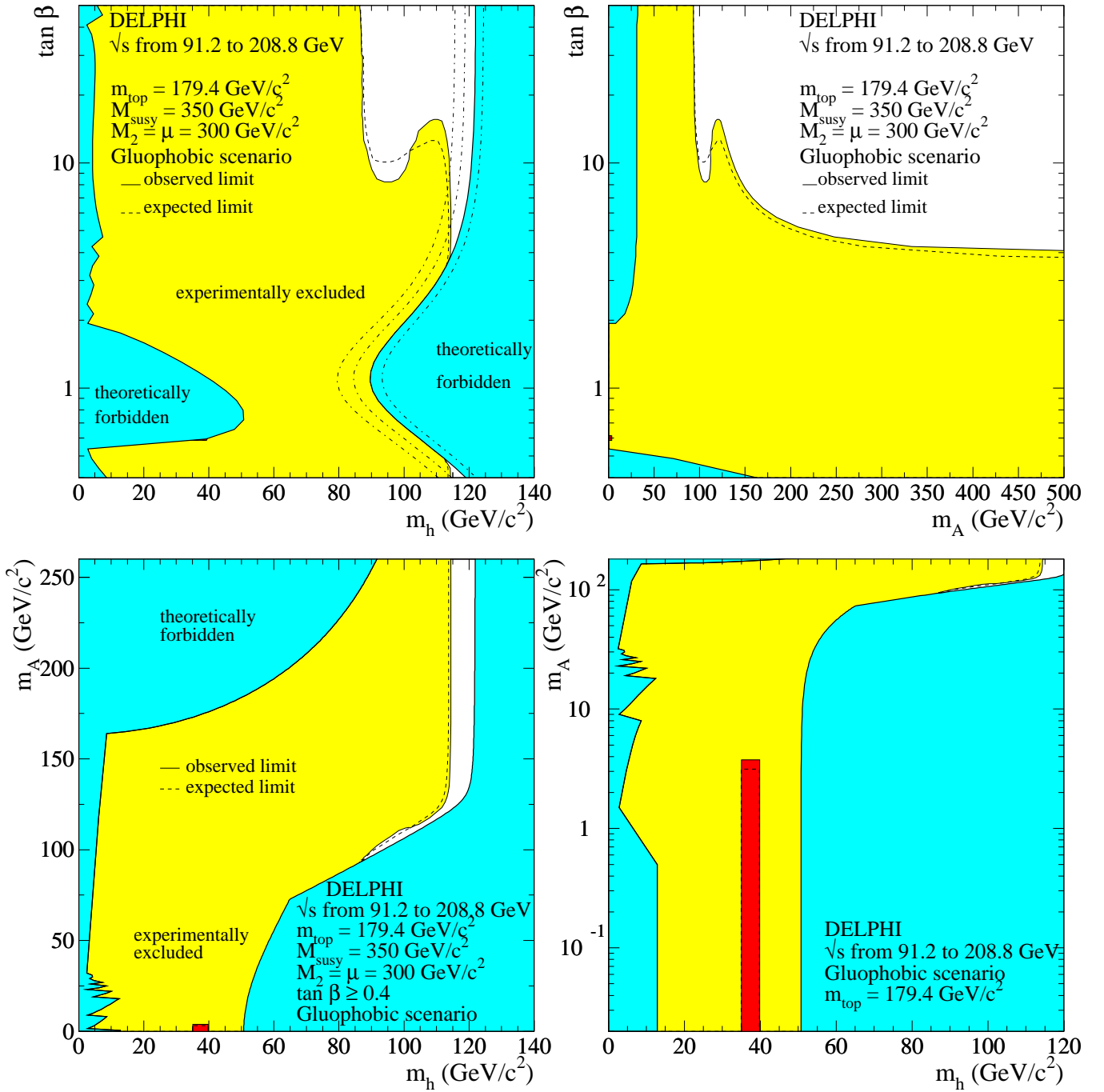


Figure 8: MSSM gluophobic scenario: regions excluded at 95% CL by combining the results of the Higgs boson searches in the whole DELPHI data sample (light shaded area). The unexcluded hole at low m_A and $\tan \beta$ around 0.6 is fully excluded by the limit on the Z partial width [32] that would be due to new physics (red). The dashed curves show the median expected limits. The dark shaded areas are the regions not allowed by the MSSM model in this scenario. Note in particular the large forbidden region in the $(m_A, \tan \beta)$ projection, due to points leading to unphysical h masses. The dash-dotted lines in the top left-hand plot are the theoretical upper bounds for a top mass of 169.2, 174.3 and 183.0 GeV/c^2 (from left to right).

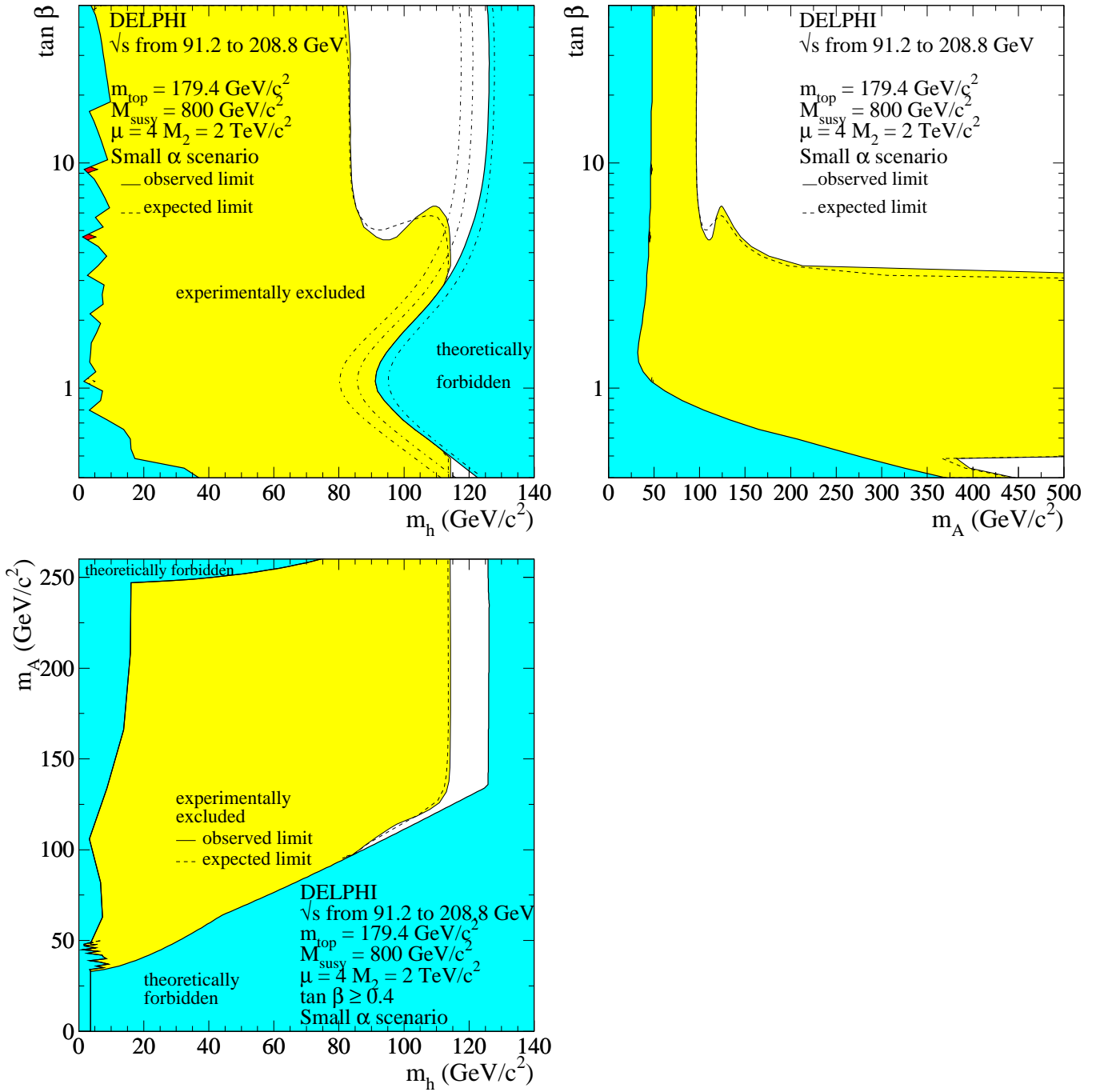


Figure 9: MSSM small α scenario: regions excluded at 95% CL by combining the results of the Higgs boson searches in the whole DELPHI data sample (light shaded area). There are a few unexcluded holes at low m_h close to the theoretical lower bound, which are all excluded by the limit on the Z partial width [32] that would be due to new physics (red). The dashed curves show the median expected limits. The dark shaded areas are the regions not allowed by the MSSM model in this scenario. Note in particular the large forbidden region in the $(m_A, \tan \beta)$ projection, due to points leading to unphysical h masses. The dash-dotted lines in the top left-hand plot are the theoretical upper bounds for a top mass of 169.2, 174.3 and 183.0 GeV/c² (from left to right).

the $h \rightarrow b\bar{b}$ branching fraction, although reduced, remains high enough (e.g. above 70% in the region where the mass limits are set) to ensure a good sensitivity. Close to the theoretical lower bound on m_h , the direct searches leave a few unexcluded islands that are all excluded by the limit on Γ^{new} .

The above results establish the following 95% CL lower limits on m_h and m_A for $m_{\text{top}} = 179.4 \text{ GeV}/c^2$:

$$m_h > 82.5 \text{ GeV}/c^2 \quad m_A > 96.5 \text{ GeV}/c^2$$

for any value of $\tan\beta$ between 0.4 and 50. The expected median limits are $81.3 \text{ GeV}/c^2$ for m_h and $95.5 \text{ GeV}/c^2$ for m_A . The observed limits in m_A and m_h are reached at $\tan\beta$ around 50, in a region where only the hA process contributes. As in the previous scenario, the h and A bosons are not degenerate in mass at large $\tan\beta$, which reflects in the significant difference between the h and A mass limits. Furthermore, for $m_{\text{top}} = 179.4 \text{ GeV}/c^2$, there is an excluded range in $\tan\beta$, between 0.5 and 3.1 (expected [0.5-2.9]) which is valid for any value of m_A between 0.02 and $1000 \text{ GeV}/c^2$.

The m_{top} dependence of the above limits is shown in Table 4 and Fig. 10. As in the previous scenario, the value of m_h at fixed m_A and $\tan\beta$ varies significantly with m_{top} in the region where the mass limits are set, which explains the variations of the latter. The H signal, being kinematically inaccessible for most values of m_{top} (see Table 3) plays no role in this scenario. Finally, the variation of the excluded range in $\tan\beta$ is due to the change in the maximal value of m_h which is reached at large m_A where m_h is very sensitive to m_{top} .

4.8 Summary

The lower bounds in mass and excluded ranges in $\tan\beta$ discussed in the previous sections are summarised in Table 4. The variation with m_{top} of the excluded ranges in $\tan\beta$ is further illustrated in Fig. 10. All lower bounds in mass are at the 95% CL, as well as each individual (either lower or upper) bound in $\tan\beta$.

scenario	limits	m_{top} (GeV/ c^2)			
		169.2	174.3	179.4	183.0
m_h^{max}	m_h (GeV/ c^2)	89.7	89.7	89.7	89.6
	m_A (GeV/ c^2)	90.4	90.4	90.4	90.4
	$\tan \beta$	0.6 - 2.4	0.7 - 1.9	0.9 - 1.4	none
m_h^{max} $\mu > 0$	m_h (GeV/ c^2)	89.6	89.6	89.5	89.6
	m_A (GeV/ c^2)	90.3	90.3	90.3	90.3
	$\tan \beta$	0.6 - 2.6	0.7 - 2.0	0.9 - 1.5	none
m_h^{max} $\mu > 0, X_t < 0$	m_h (GeV/ c^2)	89.6	89.6	89.5	89.6
	m_A (GeV/ c^2)	90.5	90.4	90.4	90.4
	$\tan \beta$	0.5 - 3.2	0.6 - 2.4	0.7 - 1.9	0.8 - 1.6
no mixing	m_h (GeV/ c^2)	112.8	90.6	90.0	89.9
	m_A (GeV/ c^2)	1000.	91.4	90.8	90.5
	$\tan \beta$	0.4 - 0.5	0.4 - 0.5	0.4 - 0.5	0.4 - 0.5
		0.8 - 0.9	0.8 - 0.9	0.8 - 0.9	0.8 - 0.9
		1.0 - 50.	1.0 - 9.6	1.0 - 5.4	1.0 - 4.3
no mixing $\mu > 0$ large M_{SUSY}	m_h (GeV/ c^2)	89.9	89.8	89.7	89.8
	m_A (GeV/ c^2)	90.8	90.6	90.4	90.3
	$\tan \beta$	0.9 - 6.9	0.9 - 4.5	0.9 - 3.4	0.9 - 3.0
Gluophobic	m_h (GeV/ c^2)	87.8	87.0	86.4	
	m_A (GeV/ c^2)	93.0	92.9	93.2	
	$\tan \beta$	0.4 - 9.7	0.4 - 5.2	0.5 - 3.7	
Small α	m_h (GeV/ c^2)	84.3	83.5	82.5	
	m_A (GeV/ c^2)	95.0	95.8	96.5	
	$\tan \beta$	0.4 - 6.0	0.4 - 4.0	0.5 - 3.1	

Table 4: 95% CL lower bounds on m_h and m_A and 95% CL upper and lower bounds in $\tan \beta$ obtained in the different CP-conserving MSSM benchmark scenarios, as a function of m_{top} . Dominant two-loop order radiative corrections are fully included in the theoretical calculations. The experimental results encompass searches for neutral and charged Higgs bosons in the whole data sample of DELPHI. $m_{\text{top}} = 183 \text{ GeV}/c^2$ was not studied in the gluophobic and small α scenarios.

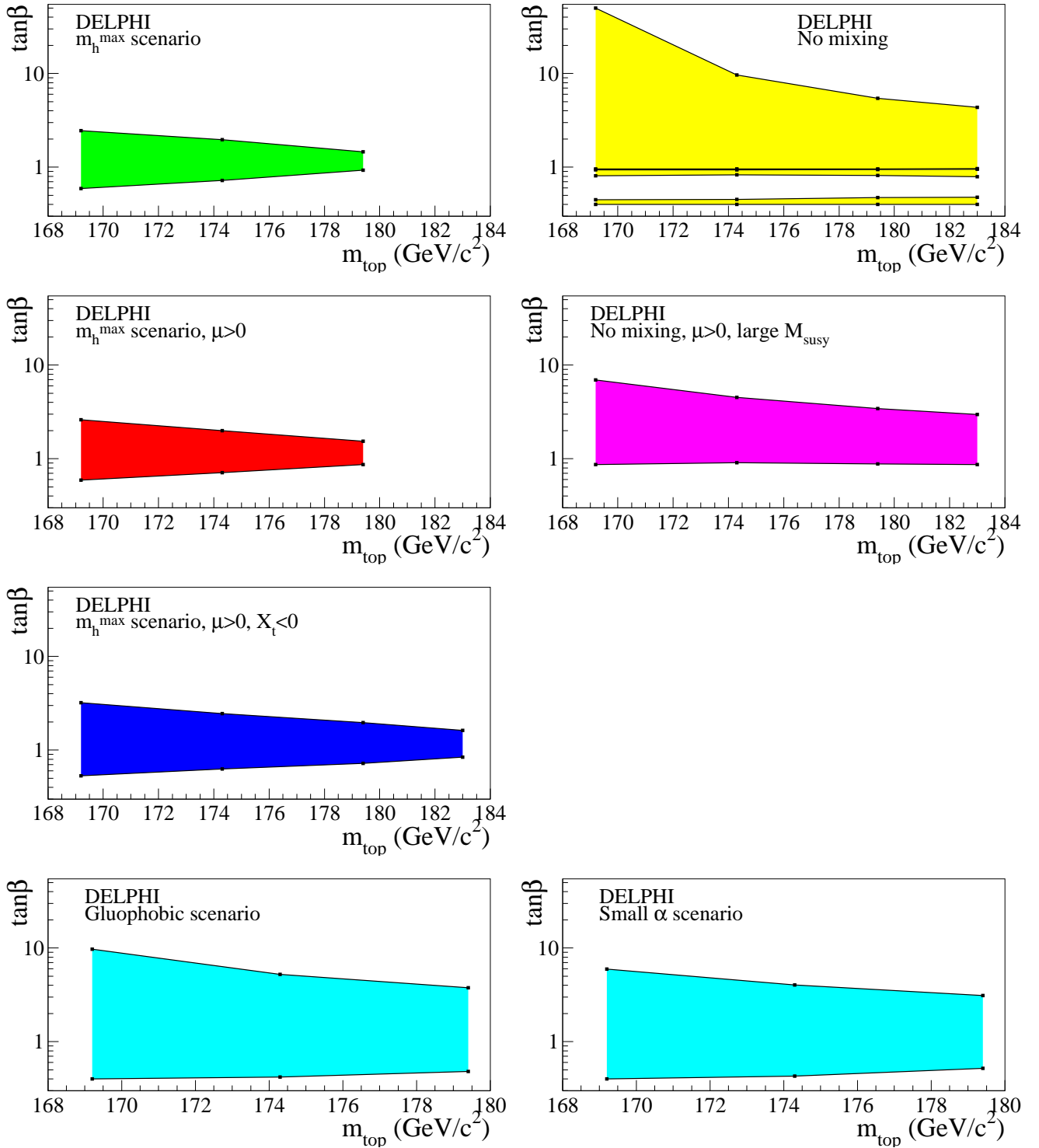


Figure 10: Variation with m_{top} of the ranges in $\tan\beta$ excluded by DELPHI in the CP-conserving MSSM benchmark scenarios. Note that each bound in $\tan\beta$ is a limit (either upper or lower) at 95% CL. $m_{\text{top}} = 183 \text{ GeV}/c^2$ was not studied in the gluophobic and small α scenarios.

5 Conclusions

Searches for neutral and charged Higgs bosons in the whole data sample of the DELPHI experiment have been combined to derive constraints on a few CP-conserving MSSM benchmark scenarios. Experimental results encompass searches for the three neutral Higgs bosons in final-states as expected in most MSSM models as well as searches for charged Higgs bosons and for neutral Higgs bosons decaying into hadrons of any flavour. The last two subsets of results bring an additional gain in sensitivity in restricted regions of the parameter space, which is covered mostly by the standard MSSM analyses. Including the production of the third neutral Higgs boson translates into a significant gain in exclusion in scenarios which makes this boson kinematically accessible at LEP.

In all benchmark scenarios, the experimental results allow to exclude a large fraction of the parameter space, even in scenarios designed to test potential difficult cases (e.g. vanishing production cross-sections or decay branching fractions) either at LEP or at hadron colliders. Limits on masses of the h and A bosons were deduced as well as upper and lower exclusion bounds in $\tan\beta$. The dependence of these limits with m_{top} was studied in a range between 169.2 to 183.0 GeV/ c^2 .

To quote but one result, the following limits at 95% of CL have been established in the framework of the m_h^{max} scenario with $m_{\text{top}} = 179.4$ GeV/ c^2 :

$$\begin{array}{llll} m_h > 89.7 \text{ GeV}/c^2 & \text{and} & m_A > 90.4 \text{ GeV}/c^2 & \text{for any } \tan\beta \text{ between } 0.4 \text{ and } 50, \\ \tan\beta < 0.9 & \text{or} & \tan\beta > 1.4 & \text{for any } m_A \text{ between } 0.02 \text{ and } 1000 \text{ GeV}/c^2. \end{array}$$

The mass limits are insensitive to variations of the top quark mass. The excluded range in $\tan\beta$ decreases with increasing m_{top} and no bound can be set on $\tan\beta$ at $m_{\text{top}} = 183.0$ GeV/ c^2 . This scenario provides the most conservative bounds on $\tan\beta$ among the eight models tested.

References

- [1] DELPHI 2004-012-CONF-688, *Updated DELPHI results on neutral Higgs bosons in MSSM benchmark scenarios*, contribution to the 2004 summer conferences.
- [2] CDF and D0 collaborations and the Tevatron electroweak working group, *Combination of CDF and D0 results on the top-quark mass*, hep-ex/0404010.
- [3] DELPHI Collaboration, P. Abreu et al., *Z. Phys.* **C51** (1991) 25
- [4] DELPHI Collaboration, P. Abreu et al., *Nucl. Phys.* **B342** (1990) 1
- [5] DELPHI Collaboration, P. Abreu et al., *Nucl. Phys.* **B373** (1992) 3
- [6] DELPHI Collaboration, P. Abreu et al., *Nucl. Phys.* **B421** (1994) 3.
- [7] S.Dagoret, PhD thesis, Universit de Paris-Sud, centre d'Orsay, LAL-preprint 91-12 (may 1991).
- [8] DELPHI Collaboration, P. Abreu et al., *Phys. Lett.* **B245** (1990) 276.
- [9] DELPHI Collaboration, P. Abreu et al., *Nucl. Phys.* **B373** (1992) 3.
- [10] DELPHI Collaboration, P. Abreu et al., *Z. Phys.* **C67** (1995) 69.
- [11] DELPHI 92-80 Dallas PHYS 191, *Neutral Higgs Bosons in a Two Doublet Model*, contribution to the 1992 ICHEP conference; quoted by G.Wormser, in proc. of the XXVI ICHEP conference (Dallas, August 1992), Vol. 2, pages 1309-14, ref. 4.
- [12] DELPHI Collaboration, P. Abreu et al., *Z. Phys.* **C73** (1996) 1.
- [13] DELPHI Collaboration, P. Abreu et al., *Eur. Phys. J.* **C2** (1998) 1.
- [14] DELPHI Collaboration, P. Abreu et al., *Eur. Phys. J.* **C10** (1999) 563.
- [15] DELPHI Collaboration, P. Abreu et al., *Eur. Phys. J.* **C17** (2000) 187, addendum *Eur. Phys. J.* **C17** (2000) 529.
- [16] DELPHI Collaboration, J. Abdallah et al., *Eur. Phys. J.* **C23** (2002) 409.
- [17] DELPHI Collaboration, J. Abdallah et al., *Eur. Phys. J.* **C32** (2004) 145.
- [18] DELPHI Collaboration, J. Abdallah et al., CERN-EP/2003-061, submitted to *E. Phys. J.*
- [19] DELPHI 2003-045-CONF-665, *DELPHI results on neutral Higgs bosons in MSSM benchmark scenarios*, contribution to the 2003 summer conferences.
- [20] DELPHI Collaboration, J. Abdallah et al., CERN-EP-PH 2004-066.
- [21] DELPHI Collaboration, J. Abdallah et al., *Eur. Phys. J.* **C34** (2004) 399.
- [22] A.L. Read, *Modified Frequentist Analysis of Search Results (The CL_s Method)*, in CERN Report 2000-005, p. 81 (2000), edited by F.James, L.Lyons and Y.Perrin.

- [23] R.D. Cousins and V.L. Highland, Nucl. Instr. and Meth. **A320** (1992) 331.
- [24] M. Carena, S. Heinemeyer, C. Wagner and G. Weiglein, *Suggestions for improved benchmark scenarios for Higgs boson searches at LEP2* CERN-TH/99-374, DESY 99-186 or hep-ph/9912223;
M. Carena, S. Heinemeyer, C. Wagner and G. Weiglein, Eur. Phys. J. **C26** (2003) 601.
- [25] DELPHI 2003-039-CONF-659, *Complete DELPHI data: Limits on Higgs Boson Masses and $\tan\beta$ from a MSSM Parameter Scan*, contribution to the 2003 summer conferences.
- [26] G. Degrandi, S. Heinemeyer, W. Hollik, P. Slavich and G. Weiglein, Eur. Phys. J. **C28** (2003) 133.
- [27] S. Heinemeyer, W. Hollik and G. Weiglein, Eur. Phys. J. **C9** (1999) 343.
- [28] M. Carena, M. Quiros and C.E.M. Wagner, Nucl. Phys. **B461** (1996) 407
M. Carena, M. Quiros and C.E.M. Wagner, Phys. Rev. **D62** (2000) 055008.
- [29] M. Carena, S. Pokorski and C.E.M. Wagner, Nucl. Phys. **B406** (1993) 59.
- [30] ALEPH, DELPHI, L3, OPAL Collaborations and the LEP Higgs working group, *Search for neutral MSSM Higgs bosons at LEP*, contribution to the 2005 summer conferences.
- [31] A.G. Akeroyd, A. Arhrib and E. Naimi, Eur. Phys. J. **C20** (2001) 51.
- [32] DELPHI Collaboration, P. Abreu et al., Eur. Phys. J. **C16** (2000) 371.